Article

Study on Flow and Heat Transfer Characteristics and Anti-Clogging Performance of Tree-Like Branching Microchannels

Linqi Shui [1,*], Zhongkai Hu [1], Hang Song [1], Zhi Zhai [2] and Jiatao Wang [1]

1 Key Laboratory of NC Machine Tools and Integrated Manufacturing Equipment of the Education Ministry, Key Laboratory of Manufacturing Equipment of Shaanxi Province, Xi'an University of Technology, Xi'an 710048, China
2 School of Mechanical Engineering, Xi'an Jiaotong University, Xi'an 710049, China; zhaizhi@xjtu.edu.cn
* Correspondence: shuilinqi@xaut.edu.cn; Tel.: +86-189-668-7925

Abstract: In this paper, a tree-like branching microchannel with bifurcating interconnections is designed for gas turbine blade cooling. A theoretical analysis, experimental study, and numerical simulation of the heat transfer and hydrodynamic characteristics of the tree-like branching microchannel is performed, and the influence of the total number of branching levels m on the anti-clogging performance is also studied. The results indicate that the total heat transfer ratio and pressure drop ratio are closely related to the structur ne parameters. The comprehensive thermal performance increase with an increase in the ratio of L_b/L_0 and fractal dimension D. Nu/Nu_s, f/f_s, and η are increased as m increases from 3 to 5. Furthermore, the tree-like microchannel network exhibits robustness for cooling gas turbine blades. A greater total number of branching levels and a higher Re number are advantageous for enhancing the anti-clogging performance of the tree-like branching microchannel.

Keywords: gas turbine cooling; tree-like branching microchannel; heat transfer characteristics; pressure drop characteristics; anti-clogging performance

1. Introduction

Virtually all modern gas turbine engines adopt high-pressure turbine components that need to be cooled with various approaches. As the cooling effectiveness rises, the temperature of the hot gas also increases, resulting in an overall increases in engine efficiency [1]. Due to the high pursuit of engine thermal efficiency and power output, the hot gas temperature has now exceeded 1800 °C, making the efficient and reliable cooling of turbine blades a severe challenge that requires an optimal cooling solution. To further increase overall cooling effectiveness, several advanced cooling technologies have been proposed and studied in recent years, including the optimization of cooling geometry parameters, the improvement of complicated cooling strategies, and the development of new cooling approaches based on innovation cooling theories [2–4]. Among these, the tree-like branching microchannel cooling technology, which possesses excellent overall heat transfer performance, has attracted the attention of researchers for blade cooling in gas turbines.

Inspired by natural tree-like branching network systems, just like tree roots, leaf veins, and mammalian blood vessels, artificial tree-like branching network systems have been designed for use in various engineering fields, including microelectronic engineering [5,6], fuel cells [7], chemical engineering [8,9], compact thermal exchangers [10,11], and thermal energy storage [12]. Bejan et al. [13,14] first proposed the "constructed theory" to guide the optimization design of microchannel sinks. West et al. [15] discussed the origin of allometric scaling laws in biology and derived the ratio of consecutive bifurcated diameters and lengths. Senn and Poulikakos [16] and Alharbi et al. [17] described the tree-like branching network by introducing fractal theory and predicted its pressure drop and heat transfer coefficient. It was indicated that compared to conventional parallel straight or serpentine

microchannels, tree-like branching microchannels show better flow and heat transfer performance. Chen et al. [18] observed that the presence of branches plays an essential role in mass transfer and chemical reaction and pointed out that the figure of merit and reaction rate in tree-like branching networks are superior to those in serpentine channels.

Numerous studies have investigated the flow and thermal properties of tree-like branching networks and their impact on cooling performance. Chen et al. [19] examined the pressure drop and heat transfer characteristics of a fractal branching channel and found that a larger total number of branching levels or a larger fractal dimension enhances heat transfer capability with a smaller pumping power penalty. They assumed laminar and fully developed flow and ignored the bifurcation effect on pressure drop. Rubio-Jimenez et al. [20] studied the effects of shape, path, and channel dimensions of tree-like microchannel networks on hydraulic and thermal performance. They observed that bifurcated microchannel networks improve heat dissipation and a geometrical channel ratio of 1.618 provides the best performance. Jing et al. [21] compared two tree-like branching channel networks under constant surface area constraint and constant volume constraint. It is indicated that convection heat transfer in both networks is independent of the diameter and diameter ratio of the channel, but it increases with the channel length, channel length ratio, branching number, and branching level. Lu et al. [22] designed a Y-shaped cooling channel with 1 to 4 branching levels to mitigate the heat from electronic chips. The results suggested that the optimal branching level of the Y-shaped channel is 4. By adopting the genetic algorithm optimization, He et al. [6] analyzed the influence rank and contribution of impact factors on the performance parameters. It was found that the optimal branching level is 4.

Taking into account the possibility of accidental damage occurring in microchannels embedded in the heat sink, Wang et al. [23,24] and Xu et al. [25] carried out a series of tests on the flow and heat transfer performance of tree-like microchannel networks while one or more subchannel segments were blocked. They concluded that the branching microchannel networks with loops can ensure the continuity of coolant flow and provide better stability in the event of an accidental blockage in subchannel segments. Miao et al. [26] pointed out that the thermal and flow transport characteristics in the damaged tree-like branching network are quite different from those in an undamaged network. In their research, the number of damaged channels and branching levels demonstrated a significant influence on the optimal diameter ratio and optimal thermal conductivity.

It is worth mentioning that most coolants adopted in previous research on cooling in branching microchannel networks have been single-phase or two-phase liquid fluid, and the coolant flows usually in laminar flow conditions. There is still limited research on the use of air coolant for cooling gas turbine blades. As a conceptual design, Devore and Kaufman [27] proposed a dendritic aerofoil core cooling arrangement to restrict the number of channel inlets and control pressure drop in the vicinity of the inlet. In the patent disclosed by Ahmad et al. [28] from Siemens AG, a cooling arrangement of bifurcated channels was revealed to maintain overall cooling effects in case of damage to the turbine blade in the region of cooling channels. Shui et al. [29,30] investigated the air and steam flow and heat transfer characteristics of Y-shaped and T-shaped tree-like microchannels with branching levels of $m = 3$ for gas turbine blade cooling.

From the foregoing discussion, it is clear that all previous air-cooling research has been based on fixed branching level conditions. Nevertheless, almost no attention was paid to air cooling characteristics under different branching level conditions. Additionally, the airflow blockage phenomenon in the bifurcated channel has not been deeply discussed. Accidental damage to one or more channel segments can contribute to a terrible working environment. Therefore, a systematic analysis concentrated on the effect of branching level and flow blockage on the transport properties of fluid flow and heat transfer characteristics would be very meaningful for the practical application of branching network cooling technology in the area of high-temperature gas turbine blades. In this paper, we will study the issues mentioned above in detail.

2. Methodology

2.1. Physical Model

Note that the tree-like branched network possesses a self-similar property, which means that new bifurcations can be generated through similar fractal rules [31]. The detailed procedure for generating a fractal, tree-like branched channel network is described as follows:

A tree-like network structure with different branching levels as demonstrated in Figure 1a, can be achieved by replicating the elementary branch presented in Figure 1b. We assume that each channel divides into two branches at the next level, with a branch number (*N*) of two, and a branched angle (*θ*) of 60°. Following this generation rule, each sub-channel bifurcates into additional channels, forming tree-like branching microchannels. The channel length ratio and hydraulic diameter ratio at level *k* + 1 to those of the nk smaller daughter branches at the next level are, respectively denoted as

$$\alpha = \frac{L_{k+1}}{L_k}, \tag{1}$$

$$\beta = \frac{d_{k+1}}{d_k}, \tag{2}$$

Thus, it is easy to get

$$L_k = L_0 \alpha^k, \tag{3}$$

$$d_k = d_0 \beta^k, \tag{4}$$

where L_0 and L_k are the channel length of the 0th and *k*th branching levels, d_0 and d_k are the channel hydraulic diameters of the 0th and *k*th branching levels, respectively.
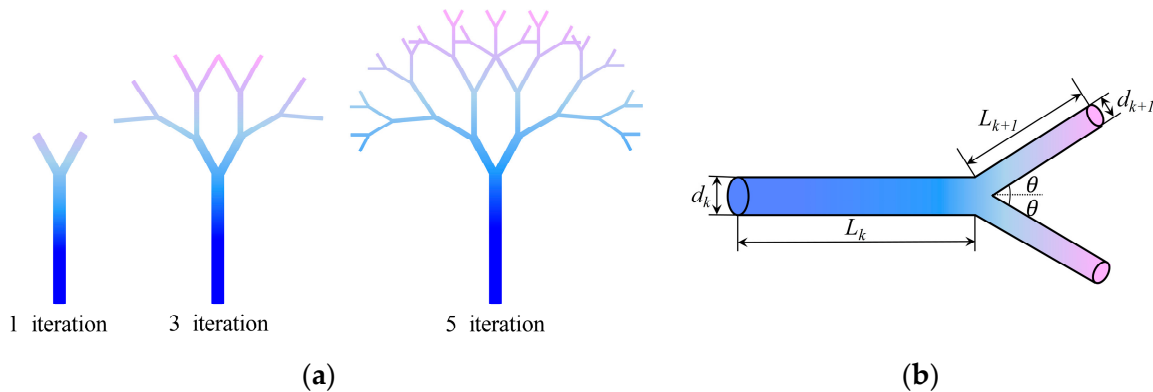

Figure 1. Sketch of (**a**) tree-like bifurcated networks and (**b**) the *k*th bifurcating level with *n* = 2.

It should be noted that the fractal dimension of the channel length distribution, *D*, and the fractal dimension of the hydraulic diameter distribution, Δ, are generated from Equations (5) and (6), respectively.

$$N = \alpha^{-D}, \tag{5}$$

$$N = \beta^{-\Delta}. \tag{6}$$

Hence,

$$\alpha = N^{-\frac{1}{D}}, \tag{7}$$

$$\beta = N^{-\frac{1}{\Delta}}. \tag{8}$$

In the process of dimensional design, we refer to Murray's law of bifurcation network system and fractal self-similarity feature. In Murray's law, the length of the vessel is used as a constant, and there is no optimization result for the length. Meanwhile, in previous reports, studies on the ratio of length have not been as extensively investigated as those on the diameter ratio. Thus, in this discussion, the length ratio is deemed the same as the diameter ratio, i.e., $\alpha = \beta$.

Based on the above relationship and starting with an initiator channel, the skeleton of the model expands by recursively applying a growth and bifurcating generator to the tips of the model. Besides, to prevent flow clogging in the microchannel at the last level, the last branches were interconnected, as shown in Figure 2.
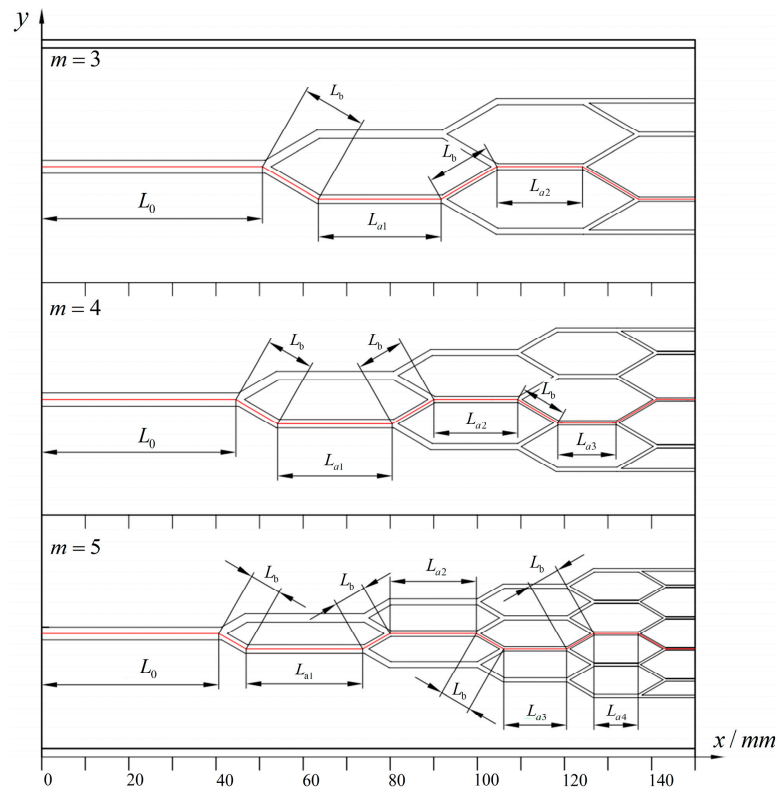

Figure 2. Two-dimensional view of the tree-like bifurcating microchannels with m = 3, 4, 5.

It is noted that the channel length of each level L_k, except for the initial channel L_0, can be split into the sum of the oblique channel length L_b and the straight channel length L_{ak}, namely, $L_k = L_b + L_{ak}$.

2.2. Heat Transfer in the Tree-like Branching Networks

The total heat transfer area of a tree-like net S with m branch levels can be characterized by the following equation

$$\begin{aligned} S &= \sum_{k=0}^{m} \left[(k+1)\pi d_k L_{ak} + 2k\pi d_k L_b \right] \\ &= \pi \sum_{k=0}^{m} \left[(k+1)L_{ak} + 2kL_b \right] \cdot d_k \end{aligned} \tag{9}$$

According to the relationship among L_k, L_b, and L_{ak} described before, that is, $L_k = L_b + L_{ak}$, Equation (9) can be simplified into Equation (10)

$$S = \pi \sum_{k=0}^{m} \left[(k+1)L_k + (k-1)L_b \right] \cdot d_k, \tag{10}$$

and substituting Equations (3) and (4) into Equation (10) yields

$$
\begin{aligned}
S \quad &= \pi \sum_{k=0}^{m} \left[(k+1)L_0\alpha^k + (k-1)L_b \right] \cdot d_0\beta^k \\
&= \pi d_o L_o \frac{1-(m+2)(\alpha\beta)^{m+1}+(m+1)(\alpha\beta)^{m+2}}{(1-\alpha\beta)^2} \\
&+ \pi d_o L_b \frac{2\beta-m\beta^{m+1}+(m-1)\beta^{m+2}-1}{(1-\beta)^2}
\end{aligned}
\tag{11}
$$

Assuming the laminar flow through each channel has reached a sufficiently developed state both hydrodynamically and thermodynamically, the *Nu* number is kept constant at each level of the bifurcation. Thus, the heat transfer coefficient of the upper-level branches will augment due to

$$
\frac{h_{k+1}}{h_k} = \frac{d_k}{d_{k+1}},
\tag{12}
$$

and substituting Equation (2) into Equation (12) gives

$$
\frac{h_{k+1}}{h_k} = \frac{1}{\beta}.
\tag{13}
$$

Sequentially,

$$
h_k = h_0\beta^{-k}.
\tag{14}
$$

A fully developed flow in an even cross-section with a constant heat flux condition results in a constant temperature difference (ΔT) between the bulk flow and the wall surface. To compare this with parallel channels, it is also assumed that the temperature variance for each bifurcating level is the same constant (ΔT) [19].

Based on Equation (11), it is easy to know that S_k can be represented as

$$
\begin{aligned}
S_k \quad &= \pi d_k[(k+1)L_k + (k-1)L_b] \\
&= \pi d_0\beta^k \left[(k+1)L_0\alpha^k + (k-1)L_b \right]
\end{aligned}
\tag{15}
$$

Consequently, the total convection heat transfer can be calculated accordingly

$$
Q_h = \sum_{k=0}^{m} h_k S_k \Delta T = \sum_{k=0}^{m} h_k \pi d_k[(k+1)L_k + (k-1)L_b]\Delta T.
\tag{16}
$$

Substituting Equations (3), (4), and (14) into Equation (16) yields

$$
\begin{aligned}
Q_h \quad &= \sum_{k=0}^{m} h_0\beta^{-k}\pi d_0\beta^k \left[(k+1)L_0\alpha^k + (k-1)L_b \right]\Delta T \\
&= \pi h_0 d_0 \sum_{k=0}^{m} \left[(k+1)L_0\alpha^k + (k-1)L_b \right]\Delta T \\
&= \pi h_0 d_0 \left[L_0 \frac{1-(m+2)\alpha^{m+1}+(m+1)\alpha^{m+2}}{(1-\alpha)^2} + L_b \frac{m^2-m}{2} \right]\Delta T
\end{aligned}
\tag{17}
$$

In the case of a parallel channel network with diameter d_0, under the identical heat transfer area, temperature variance and *Nu* number conditions, the total convection heat transfer is

$$
Q_{hp1} = h_0 S \Delta T.
\tag{18}
$$

Substituting Equation (15) into Equation (18) gives

$$
\begin{aligned}
Q_{hp1} = \quad &\pi d_o h_0 \left[L_o \frac{1-(m+2)(\alpha\beta)^{m+1}+(m+1)(\alpha\beta)^{m+2}}{(1-\alpha\beta)^2} \right. \\
&\left. + L_b \frac{2\beta-m\beta^{m+1}+(m-1)\beta^{m+2}-1}{(1-\beta)^2} \right]\Delta T
\end{aligned}
\tag{19}
$$

Therefore, the ratio of Q_h/Q_{hp1} is

$$\frac{Q_h}{Q_{hp1}} = \frac{\frac{1-(m+2)\alpha^{m+1}+(m+1)\alpha^{m+2}}{(1-\alpha)^2} + \frac{L_b}{L_0}\frac{m^2-m}{2}}{\frac{1-(m+2)(\alpha\beta)^{m+1}+(m+1)(\alpha\beta)^{m+2}}{(1-\alpha\beta)^2} + \frac{L_b}{L_0}\frac{2\beta-m\beta^{m+1}+(m-1)\beta^{m+2}-1}{(1-\beta)^2}},$$

(20)

where denoted by Equation (7) is a function of D and N, while denoted by Equation (8) is a function of N and Δ.

As shown in Equation (20), the ratio of Q_h to Q_{hp1} is dependent on both α, β, and L_b/L_0. Thus, Equation (20) was calculated for $N = 2$, $\Delta = 2$, $D = 3$, $m = 3, 4, 5$, and $L_b/L_0 = 0.1\text{–}1$, and the results are illustrated in Figure 3a. Also, it was computed for $\Delta = 3$, $N = 2$, $L_b/L_0 = 0.2344$, $m = 3, 4, 5$, and $D = 1\text{–}3.5$, and the corresponding results are presented in Figure 3b. It is presented that the tree-like branching microchannels show a superior heat transfer performance than those of the conventional parallel microchannels. Moreover, the larger the ratio of L_b/L_0, the total number of the bifurcating levels m, or the fractal dimension D, the larger the heat transfer performance.
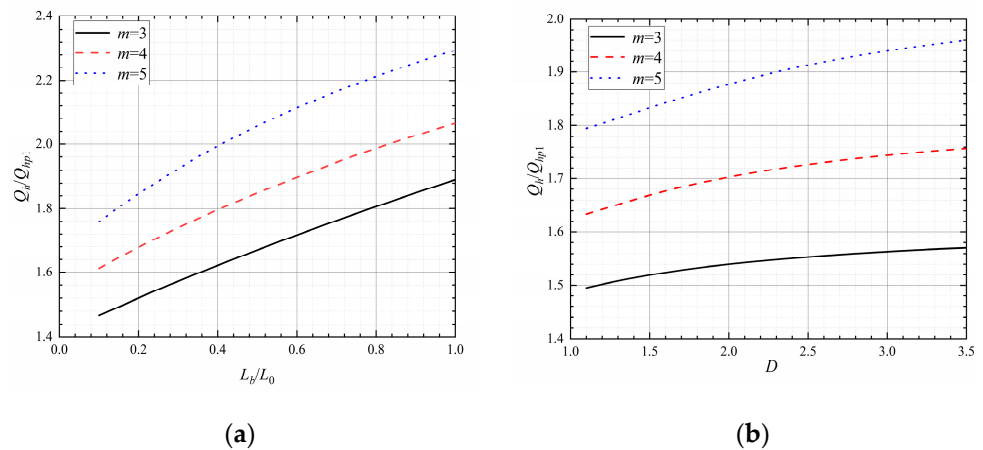

(a)   (b)

Figure 3. Plot of Q_h/Q_{hp1} versus (**a**) L_b/L_0 at $N = 2$, $\Delta = 2$, $D = 3$, $m = 3, 4, 5$, and (**b**) D at $\Delta = 3$, $N = 2$, $L_b/L_0 = 0.2344$, $m = 3, 4, 5$.

2.3. Flow Resistance in the Tree-like Branching Networks

Disregarding the effects of bifurcation and confluence, the pressure drop of a fully developed laminar flow through the nets of tree-like bifurcating channels can be stated as

$$\Delta p_f = \sum_{k=0}^{m} \frac{c}{d_k^2}((k+1)L_k + (k-1)L_b)v_k,$$

(21)

where v_k denotes the velocity in the channel with the kth branching level and c represents a constant. Based on the law of mass conservation, we can obtain

$$v_k d_k^2 N^k = v_0 d_0^2$$

(22)

and thus

$$v_k = v_0\left(\frac{d_0}{d_k}\right)^2 \frac{1}{N^k}.$$

(23)

Substituting Equation (23) into Equation (21) yields

$$\Delta p_f = \sum_{k=0}^{m} \frac{c}{d_0^2}((k+1)L_k + (k-1)L_b)\frac{v_0}{\beta^{4k}N^k}.$$

(24)

The inlet flow rate Q can be defined as

$$Q = v_0 \frac{\pi}{4} d_0^2, \tag{25}$$

and the required total pumping power is

$$P = Q\Delta p_f. \tag{26}$$

Substituting Equations (1), (2), (24), and (25) into Equation (26) yields

$$
\begin{aligned}
P &= \frac{\pi}{4} v_0 d_0^2 \left[\sum_{k=0}^{m} \frac{cv_0}{d_0^2} ((k+1)L_k + (k-1)L_b) \frac{1}{\beta^{4k} N^k} \right] \\
&= \frac{\pi c}{4} v_0^2 \left(L_o \frac{1 - (m+2)\left(\alpha/\left(\beta^4 N\right)\right)^{m+1} + (m+1)\left(\alpha/\left(\beta^4 N\right)\right)^{m+2}}{\left(1 - \alpha/\left(\beta^4 N\right)\right)^2} \right. \\
&\quad \left. + L_b \frac{2/\left(\beta^4 N\right) - m/\left(\beta^4 N\right)^{m+1} + (m-1)/\left(\beta^4 N\right)^{m+2} - 1}{\left(1 - 1/\left(\beta^4 N\right)\right)^2} \right).
\end{aligned} \tag{27}
$$

Then, to compare the pressure drop through the network of the tree-like bifurcating channel with that of a conventional parallel network, it is under the condition that the parallel channel net possesses the identical inlet flow rate, the temperature variance, and the heat transfer rate as the tree like bifurcating channel. Therefore,

$$S_{p2} = L\pi dn, \tag{28}$$

$$Q_{hp2} = hS_{p2}\Delta T = Q_h, \tag{29}$$

where S_{p2} represents the convection heat transfer area of the parallel net, d denotes the channel diameter, L equals L_0, and n represents the number of channels. Assuming that the flow through parallel channel possesses the identical Nu number as that in the tree-like bifurcating channel, we can obtain $hd = h_0 d_0$. Then, substituting Equations (17) and (28) into Equation (29) yields

$$n = \frac{1 - (m+2)\alpha^{m+1} + (m+1)\alpha^{m+2}}{(1-\alpha)^2} + \frac{L_b(m^2 - m)}{2L_0}, \tag{30}$$

The pressure drop as well as the coolant flow rate through the parallel channels are defined as follows

$$\Delta p_{p2} = \frac{c}{d^2} L_0 v_0, \tag{31}$$

$$Q_{p2} = \frac{\pi}{4} v_0 d^2 n, \tag{32}$$

Thus, the required pumping power is

$$P_{p2} = Q_{p2}\Delta p_{p2}. \tag{33}$$

Combining Equations (31)–(33) gives

$$P_{p2} = \frac{\pi}{4} c L_0 v_0^2 n. \tag{34}$$

With the aid of Equation (30), Equation (34) can be evolved into

$$P_{p2} = \frac{\pi c}{4} v_0^2 L_0 \left[\frac{1 - (m+2)\alpha^{m+1} + (m+1)\alpha^{m+2}}{(1-\alpha)^2} + \frac{L_b(m^2 - m)}{2L_0} \right]. \tag{35}$$

Consequently, the ratio of P/P_{p2} follows

$$
\frac{P}{P_{p2}} = \frac{\dfrac{1-(m+2)\left(\alpha/\left(\beta^4 N\right)\right)^{m+1}+(m+1)\left(\alpha/\left(\beta^4 N\right)\right)^{m+2}}{\left(1-\alpha/\left(\beta^4 N\right)\right)^2}}{\dfrac{1-(m+2)\alpha^{m+1}+(m+1)\alpha^{m+2}}{(1-\alpha)^2}+\dfrac{L_b\left(m^2-m\right)}{2L_0}} + \frac{\dfrac{L_b}{L_o}\dfrac{2/\left(\beta^4 N\right)-m/\left(\beta^4 N\right)^{m+1}+(m-1)/\left(\beta^4 N\right)^{m+2}-1}{\left(1-1/\left(\beta^4 N\right)\right)^2}}{\dfrac{1-(m+2)\alpha^{m+1}+(m+1)\alpha^{m+2}}{(1-\alpha)^2}+\dfrac{L_b\left(m^2-m\right)}{2L_0}}.
\tag{36}
$$

As shown in Equation (36), it can be concluded that the ratio P/P_{p2} of is not only related to α and β, but also to the L_b/L_0.

Equation (36) was calculated for $N = 2$, $\Delta = 3$, $D = 2$, $m = 3, 4, 5$ and $L_b/L_0 = 0.1$–1. The results are shown in Figure 4a. It illustrates that the tree-like bifurcating network requires much lower pumping power than a parallel network. Additionally, as the ratio of L_b/L_0 or the total number of branching levels m augments, the required pumping power also increases. Figure 4b exhibits the computed results of Equation (36) for $\Delta = 3$, $N = 2$, $L_b/L_0 = 0.239$, $m = 3, 4, 5$ and $D = 1$–3.5. It is evident that the necessary pumping power in the channel varies depending on the value of D, which represents the length fractal dimension. As the value of D and m increase, the requisite pumping power throughout the flow channel also increases.
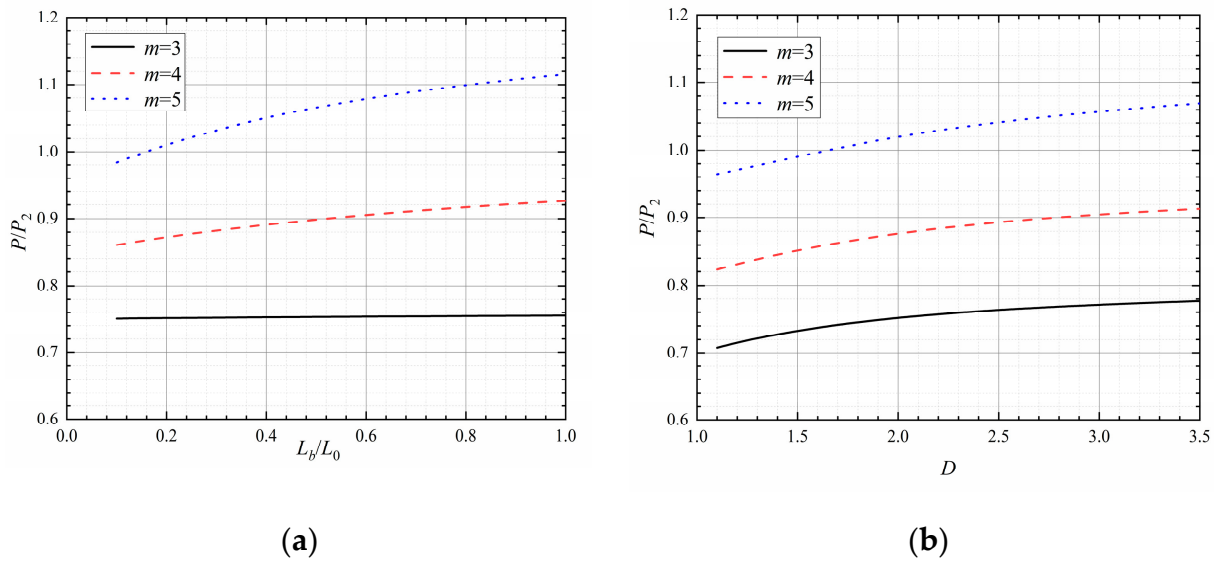

(a)　　　　　　　　　　　　　　　　　　　**(b)**

Figure 4. Plot of P/P_{p2} versus (**a**) L_b/L_0 at $\Delta = 3$, $N = 2$, $D = 2$, $m = 3, 4, 5$, and (**b**) D at $N = 2$, $\Delta = 3$, $L_b/L_0 = 0.239$, $m = 3, 4, 5$.

3. Numerical Approach and Experimental Details

3.1. Numerical Approach

To acquire a thorough understanding of the intricate flow and heat transfer characteristics in tree-like microchannels with different bifurcating levels, three dimensional steady-state numerical simulations were executed. The models' geometries are shown in Figure 2, and detailed geometrical parameters are listed in Table 1. Figure 5 exhibits the solution models and numerical grids in detail. A static temperature of 303 K and a turbulent intensity of 5% were applied at the inlet domain. The *Re* number ranged from 1000 to 20,000 and was controlled by the inlet velocity. A static back pressure was exerted at the outlet region. The bottom wall was regarded as the heating surface with a constant heat flux of 6000 W/m^2, while the other walls were set to be adiabatic with non-slip velocity conditions.

Table 1. The geometric parameters of tree-like microchannels.

k	m = 3			m = 4			m = 5		
	l_k/mm	d_k/mm	W_k/mm	l_k/mm	d_k/mm	W_k/mm	l_k/mm	d_k/mm	W_k/mm
0	50.67	3	3	44.56	3	3	40.64	3	3
1	43	2.38	1.97	35.37	2.38	1.97	32.25	2.38	1.97
2	34.44	1.89	1.38	28.07	1.89	1.38	25.6	1.89	1.38
3	27.85	1.5	1	22.28	1.5	1	20.31	1.5	1
4	-	-	-	17.68	1.19	0.74	16.12	1.19	0.74
5	-	-	-	-	-	-	12.8	0.945	0.56
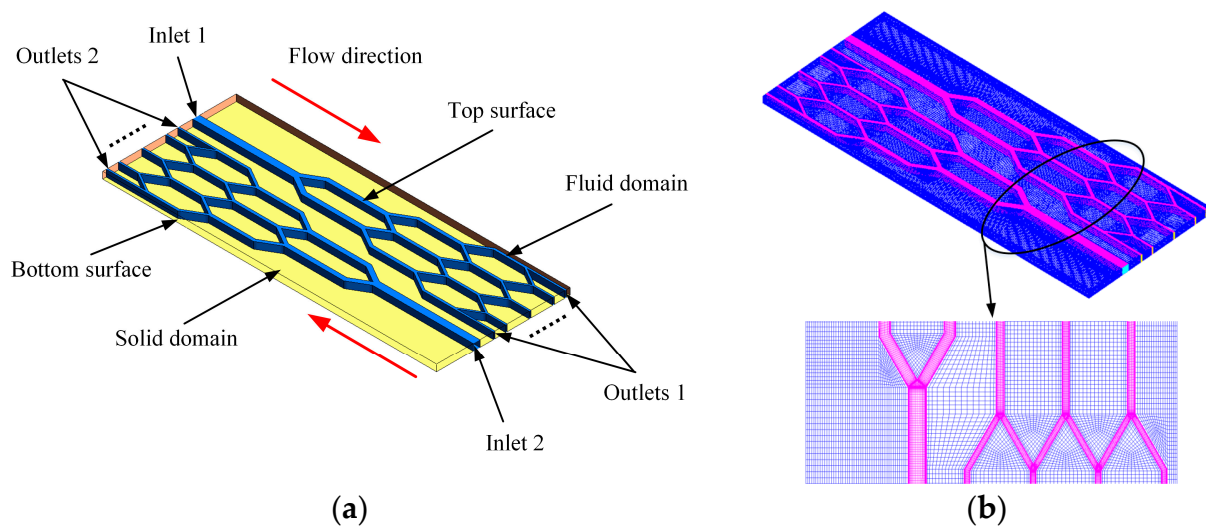
Figure 5. Schematic view of the (**a**) solution domain and (**b**) grids.

Numerical computations were performed using the fully implicit control-volume method with the high-resolution advection scheme and turbulence numerics in the CFD package, ANSYS CFX V20.0. The calculations converged to 1×10^{-5}. The reliability of the computations depends strongly on the choice of the turbulence model, with each model being suitable for different flow patterns. In the case of branching and intersecting flow computations, the selection of an appropriate turbulent flow model is crucial. The SSG turbulence model has been shown to accurately predict the complex features and physics of secondary flow in branching microchannel networks by Shui et al. [29,30], and was therefore chosen for this study. Therefore, the SSG turbulence model was selected in this study. Moreover, a scalable wall function was applied to near-wall modeling.

As depicted in Figure 5b, the computational domain grid was discretized into fine cells for conducting numerical analysis. Local grid refinement was implemented for all cases, and the *y* plus value for the first point near the wall was predominately around 1. To guarantee computation accuracy, the grid independence of various structures was verified. For the cases of *m* = 3, 4, and 5, the appropriate grid sizes fell in the range of 3.50 million, 1.12 million, and 5.24 million, respectively.

3.2. Experimental Details

A schematic representation of the experimental platform used for the microchannel cooling test is given in Figure 6. The facility consisted primarily of a test section with tree-like bifurcating microchannels, an air compressor, a heating apparatus, and a data acquisition and control system. A comprehensive explanation of the experimental process can be discovered in the literature [29].
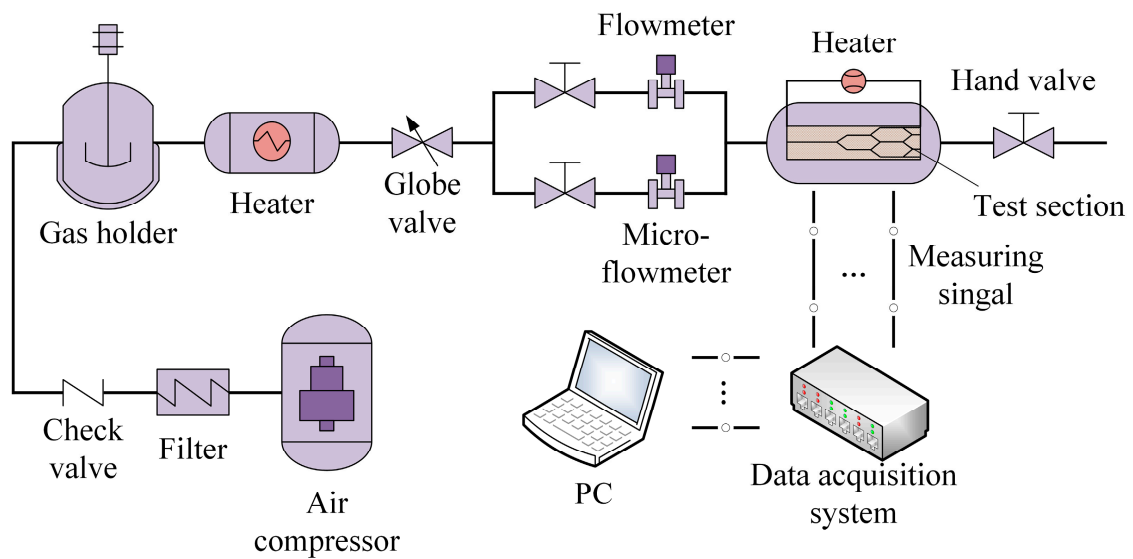
Figure 6. Schematic diagram of the cooling experimental platform.

　　　The T2 copper test section was made up of two parts: a 1 mm thick cover plate and a 5 mm thick substrate. The tree-like branching microchannel networks were micro-milled out of the substrate using high-precision processing equipment. The cover plate had the same dimensions of the substrate but without micro-milling. The two parts were assembled and sealed by tin soldering. Figure 7 shows photos of three substrates.
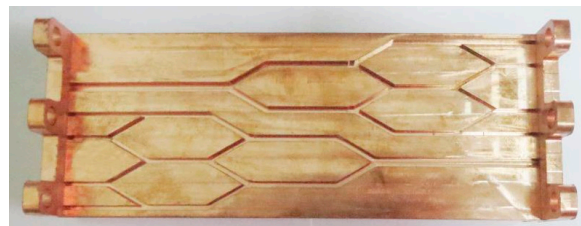
(**a**)
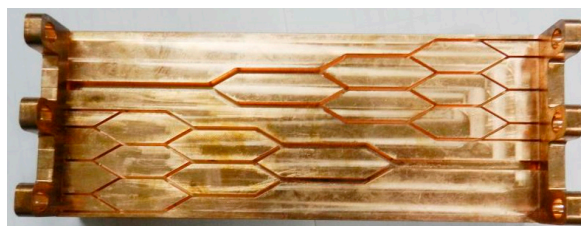
(**b**)

(**c**)

Figure 7. Photos of the copper substrate for (**a**) $m = 3$, (**b**) $m = 4$, and (**c**) $m = 5$.

To take a measurement for the wall temperature of the tree-like bifurcating microchannels, calibrated J-type thermocouples were adhered to the outer surface of the cover plate. As shown in Figure 8, 22, 24, and 24 thermocouples are decorated along the projection center lines of the bifurcating microchannel for *m* = 3, 4, and 5, respectively.
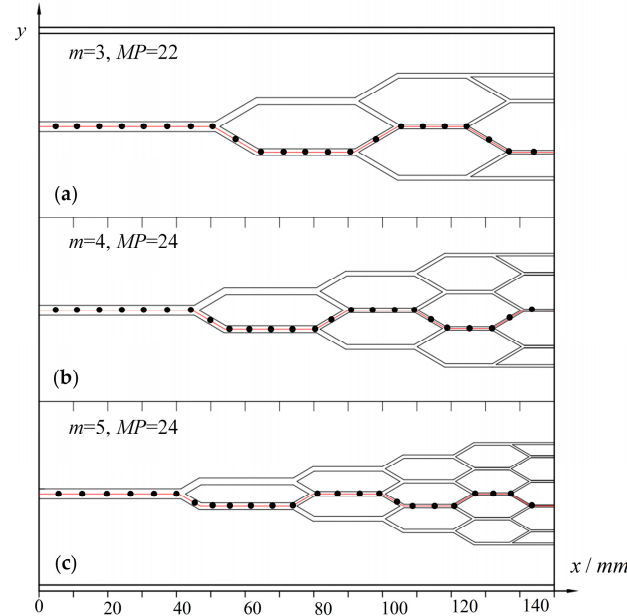

Figure 8. The layout of thermocouples measuring points (*MP*) for (**a**) *m* = 3, (**b**) *m* = 4, and (**c**) *m* = 5.

A detailed schematic of the test section is presented in Figure 9. It is worth noting that the actual absolute temperature ratio of main gas flow to cooling air, as observed in the Mitsubishi Heavy Industries gas turbine M701F, is 0.4193. However, achieving this precise heating condition in the experimental system is challenging. Therefore, the temperature ratio range is expanded, as demonstrated in the gas turbine blade cooling test bench developed by Allison Co. Ltd. [32]. In this test bench, the temperature ratio range is between 0.65 and 0.85. In the present work, the film heater had a 150 mm × 60 mm heating area and was fixed at the bottom of the substrate to ensure uniform heating. The heat flux was adjusted experimentally through an AC power source, with a range of 10 to 100 W, resulting in heat flux values ranging from 1111 to 11,111 W/m². The temperature ratio varied between 0.68 and 0.89, depending on the flow and heating conditions.
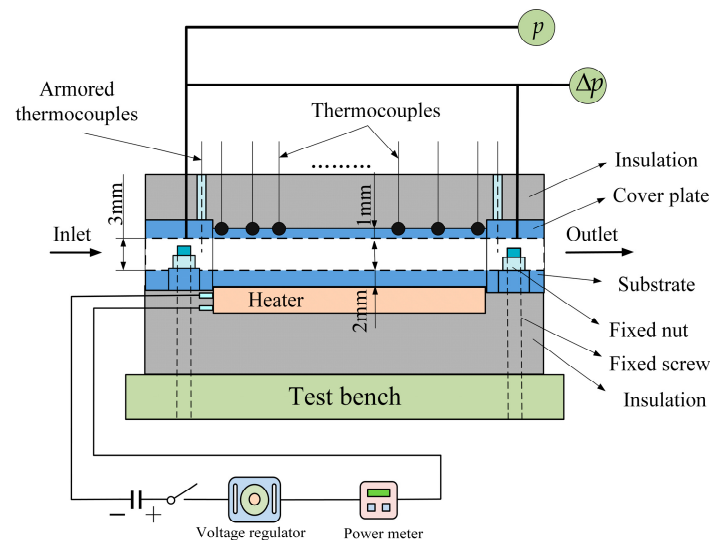

Figure 9. Design of the test section.

3.3. Data Reduction

To analyze the flow characteristics, the non-dimensional number, i.e., the inlet *Re* number, is given by

$$Re = \frac{u_{in}d_0}{\nu},$$ (37)

where ν denotes the kinematic viscosity of the coolant air, while u_{in} and d_0 are the entrance velocity and hydraulic diameter, respectively.

To evaluate the heat transfer performance, the *Nu* number is defined as

$$Nu = \frac{hd_0}{\lambda},$$ (38)

where λ is the mass-averaged thermal conductivity of coolant air and h denotes the heat transfer coefficient, which is obtained by

$$h = \frac{\dot{Q}}{A\left(T_w - T_f\right)},$$ (39)

where T_w and T_f are the wall temperature and the coolant temperature, respectively. The local wall temperature (T_w) used in Equation (39) can be read from the output of the J-type thermocouples. It was assumed that the air temperature rise along the flow duct is linear. The bulk mean temperature of air (T_f) at the l position was calculated by the following equation

$$T_f = T_{in} + \frac{l}{L}(T_{out} - T_{in}),$$ (40)

where, T_{out} and T_{in} are the air mean temperature of the outlet and inlet in the branching microchannel, respectively. l is the distance of the air flowing through the channel, and L is the centerline length from the inlet to outlet.

$\dot{Q}$ is the total heat removed by air and is estimated by

$$\dot{Q} = \rho\dot{V}c_p(T_{out} - T_{in}).$$ (41)

where ρ and $\dot{V}$ are the density and channel volume flow rate of air, respectively. The pressure loss Δp across the microchannel is defined as Equation (42), and a dimensionless pressure loss, the Fanning friction factor f, is calculated by Equation (43)

$$\Delta p = p_{in} - p_{out},$$ (42)

$$f = \frac{\Delta p}{2\rho u_{in}^2}\frac{D}{L},$$ (43)

where p_{in} and p_{out} are the pressure at the inlet and outlet of the channel, using differential pressure and adiabatic pressure sensors for measurement, respectively.

To accurately assess the comprehensive thermal performance of the complicated microchannel, the thermal enhancement factor can be expressed by

$$\eta = \frac{Nu/Nu_s}{(f/f_s)^{1/3}}.$$ (44)

Here Nu_s is the averaged *Nu* number in a smooth microchannel acquired from Stephan et al. [33] as

$$Nu_s = 4.364 + \frac{0.086(RePrd/L)^{1.33}}{1 + 0.1Pr(Red/L)^{0.3}}.$$ (45)

The friction factor in the smooth channel obtained is provided as

$$f_s = 0.315/\text{Re}^{0.25}. \tag{46}$$

The experimental uncertainties were determined using a conventional method of uncertainty analysis [34]. The uncertainties, at a 95% confidence level, are $\pm 12.8\%$ for the *Nu* number and $\pm 7.8\%$ for the flow friction factor, respectively.

4. Results

4.1. Experimental Results and Numerical Verification

Figure 10 shows the average *Nu* number versus the *Re* number of the tree-like bifurcating microchannel for *m* = 3, 4, and 5. The correlations of Stephan [33], Shah [35], Dittus-Boelter, Sieder-Tate [36], and Hausen [37] are plotted to contrasted with the experimental and numerical results. It is visible that the heat transfer performance rises with the total number of bifurcating levels over the studied *Re* number from 800 to 20,000. All the numerical values agree well with the experimental data, but they are slightly higher. The maximum deviation for *m* = 3, 4, and 5 are 15.7%, 18.8%, and 19.7%, respectively. The heat transfer coefficients of the branching networks obtained in this study are generally lower than the values computed from the correlations owing to the significant wall heat conduction and strong conjugate heat transfer effect in the microchannel. When the *Re* number exceeds 10,000, both the values of the experimental and numerical match well with the correlations of Stephan and Shah.
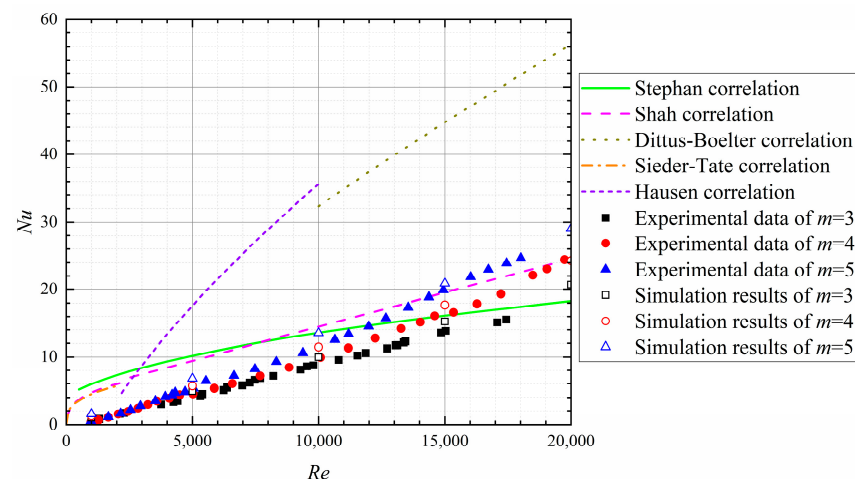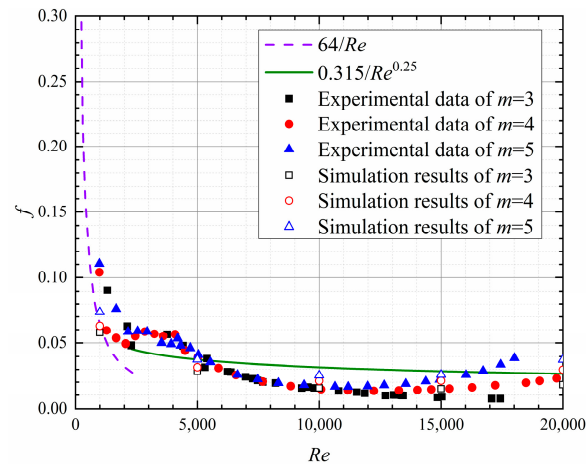

Figure 10. Comparison of experimental results, numerical data, and correlations for the average *Nu* number of tree-like branching microchannels with *m* = 3, 4, 5.

Figure 11 demonstrates the flow friction factors of tree-like bifurcating microchannels for *m* = 3, 4, and 5 obtained from both the experiment and numerical simulations, as well as the correlations of $f = 64/Re$ for $Re < 2300$ and $f = 0.315/Re^{0.25}$ for $Re > 2300$. It can be detected that the numerical values significantly increase with *m* across the studied flow conditions. However, the changing trend of *f* versus *m* for the experimental data in the laminar and transition flow regions appears irregular, possibly due to measurement errors. In the flow region where $4000 < Re < 11,000$, the influence of *m* on the flow friction factor is minimal. Nonetheless, the flow friction factors at *m* = 5 and 4 display remarkable growth as the *Re* number continues to increase, which is owed to the local flow resistances rising significantly on account of the effect of the branch confluence. In general, the values of *f* in the tree-like bifurcating microchannels exhibit similar trends in variation to the classical correlation curves at $Re < 11,000$, namely, *f* decreases as *Re* increases. However, the results of the study show a quite different and increasing tendency after that.

To test the credibility of the theory analysis, the heat flow was calculated from Equation (17). In the equation, the temperature difference ΔT corresponded with the value mea-

sured in the experiment. The pressure drop was computed from Equation (27) in which the constant *c* is set as 0.1. As shown in Figure 12a,b, the calculated results were compared to the relevant experimental data. It is clear that in both the heat flow and pressure drop through the tree-like bifurcating microchannel, the values of theory analysis are well in agreement with the experimental values. Furthermore, the experimental values, except in a small range, are larger than the theoretical calculated values, but the deviations remain at ±25%.

Figure 11. Comparison of experimental results, numerical data, and correlations for the fiction factors of tree-like branching microchannels with *m* = 3, 4, 5.
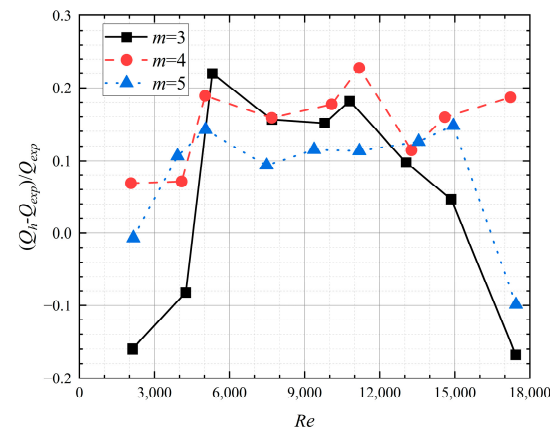
(**a**)
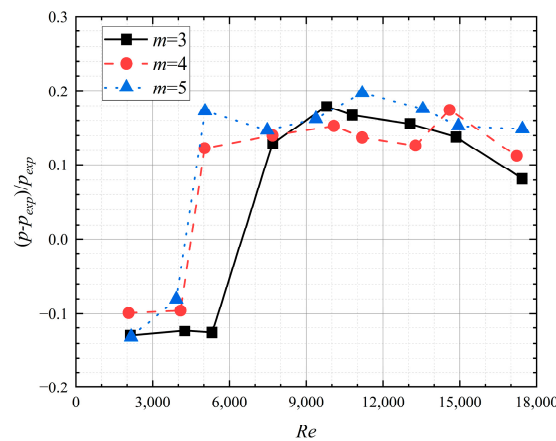
(**b**)

Figure 12. Comparison between the theoretical values and experimental data of (**a**) heat flow and (**b**) pressure drop.

4.2. Flow and Heat Transfer in Tree-like Bifurcating Microchannels

Figure 13 displays the velocity contours over the mid-plane of the tree-like branching micrchannels for m = 3, 4, and 5 at *Re* = 10,000. It can be inferred that the velocity profiles in the three planes exhibit similar distributions. The flow deflection caused by channel bifurcation and the flow acceleration introduced by channel confluence are noticeable. At an inlet velocity of 50.2 m/s, the average outlet velocities of the cases for m = 3, 4, and 5 drop down to 44.2 m/s, 48.1 m/s, and 53.7 m/s, respectively, after flowing through the bifurcated microchannel. It is suggested that as m increases, the flow acceleration and disturbance phenomena in the smaller sub-segment channels become more prominent.
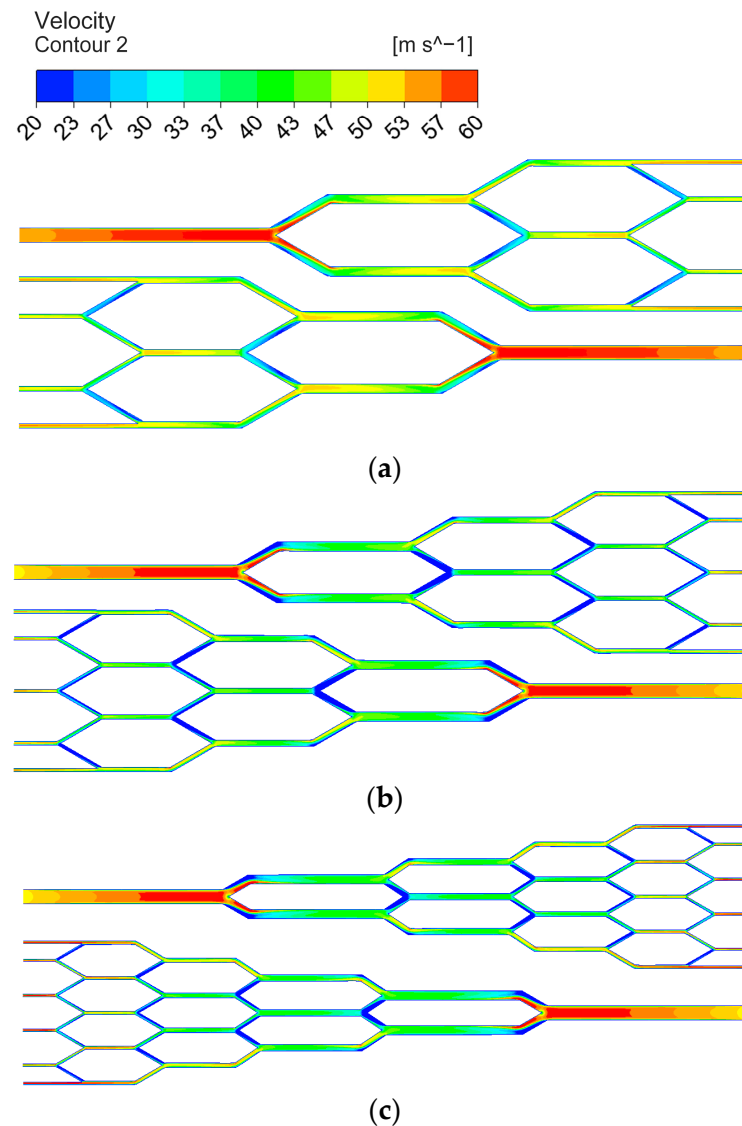

Figure 13. Velocity contour distribution over mid-plane (z = 0.5H) for (**a**) m = 3, (**b**) m = 4, and (**c**) m = 5 at *Re* = 10,000.

As depicted in Figure 14, bifurcation and confluence induce disturbed flow patterns that have been observed to greatly enhance the heat transfer in the tree-like bifurcating microchannels. In the area covered by a branching microchannel network, the heat sink is adequately cooled, and the wall temperature distribution appears relatively uniform. The maximum temperature difference over the mid-plane of the cases for m = 3, 4, and 5 is 56.1 K, 55.5 K, and 53.7 K, respectively. This does not appear to be a significant difference.
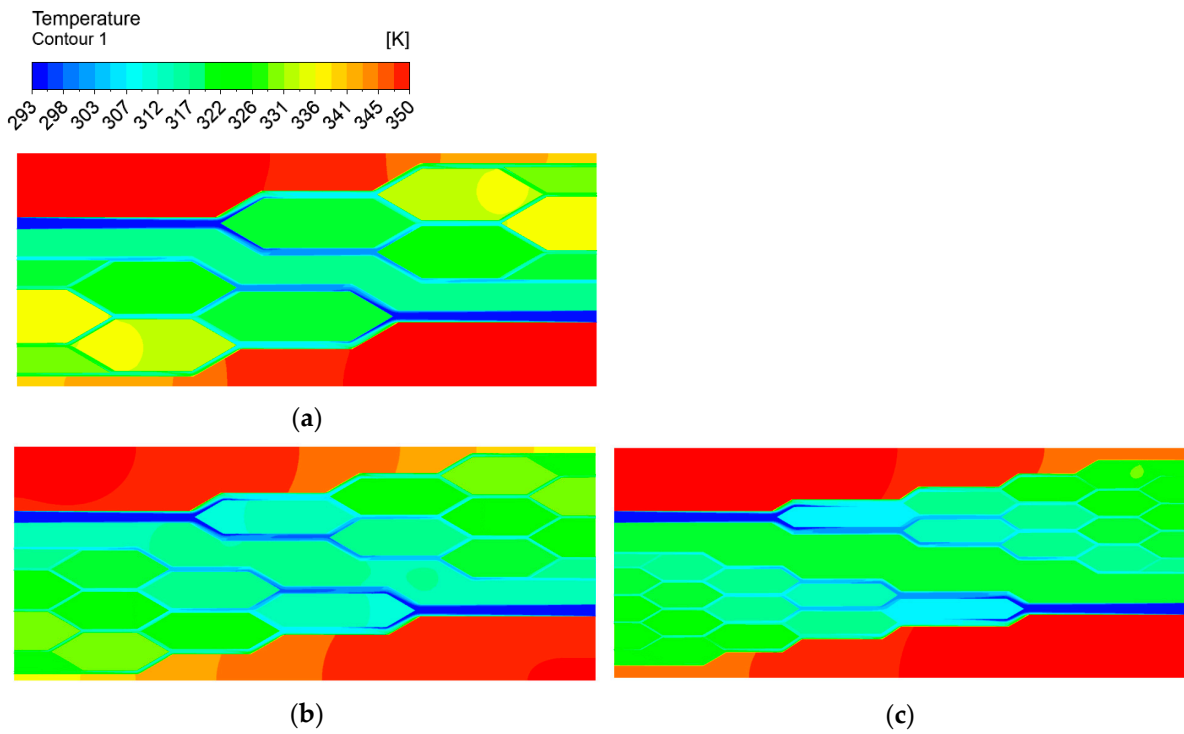
Figure 14. Temperature contour distribution over mid-plane ($z = 0.5H$) for (**a**) $m = 3$, (**b**) $m = 4$, and (**c**) $m = 5$ at $Re = 10,000$.

4.3. Thermal Enhancement Performance

Not only is it fascinating to evaluate the heat transfer capability of the tree-like bifurcating microchannel, but also intriguing to quantify the extent of thermal enhancement relative to *m*. Figure 15 plots the variation of the average *Nu* number ratios with *Re* number. It can be seen that the Nu/Nu_s tends to rise with the increasing of the *Re* number. The rising slope is steeper for $Re < 5000$, and becomes gentler for $Re = 5000$–20,000. The maximum Nu/Nu_s is obtained for $m = 5$, while the lowest is for $m = 3$. For $m = 3$, 4, and 5, the increases in Nu_a/Nu_s values are approximately 0.20, 0.25, and 0.32 at the lowest *Re* number, and 0.56, 0.79, and 1.06 at the highest *Re* number, respectively.
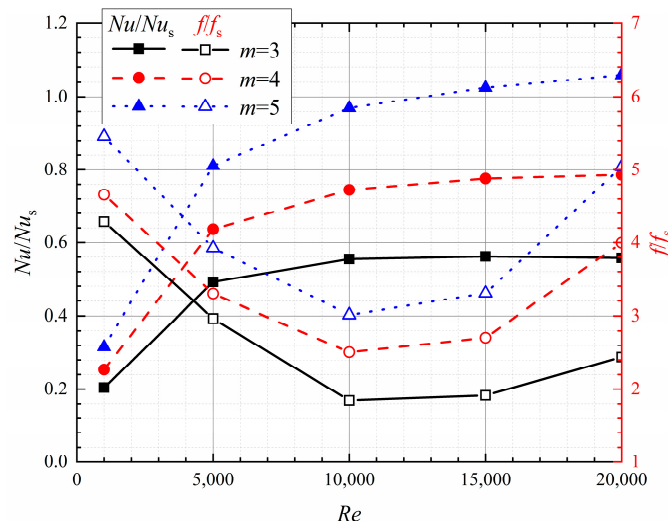

Figure 15. Variation of average *Nu* number ratio and friction factor ratio with *Re* number.

In Figure 15, the flow friction factor ratio for the same branching levels are also depicted. The friction factor ratio is increased as the channel branching level increases. It is

because the heat transfer augmentation in the tree-like bifurcating microchannel is typically accompanied by an enhancement in flow resistance. All the curves of f/f_s initially decline with the increase of Re number, and then gradually rise. At $Re = 10,000$, the lowest values of 0.49, 0.67, and 0.80 are obtained for $m = 3$, 4, and 5, respectively.

By taking into account the increment in average Nu number and f, the thermal enhancement factor η of the tree-like bifurcating microchannel can be determined. Figure 16 demonstrates the changes in the thermal enhancement factor with m. It is found that the η tends to increase when $Re < 10,000$, after which the curves level off until $Re = 15,000$. Beyond this point, all the values show a decreased trend. The variation ranges of η for $m = 3$, 4, and 5 are 0.20–0.70, 0.24–0.86, and 0.29–1.06, respectively.
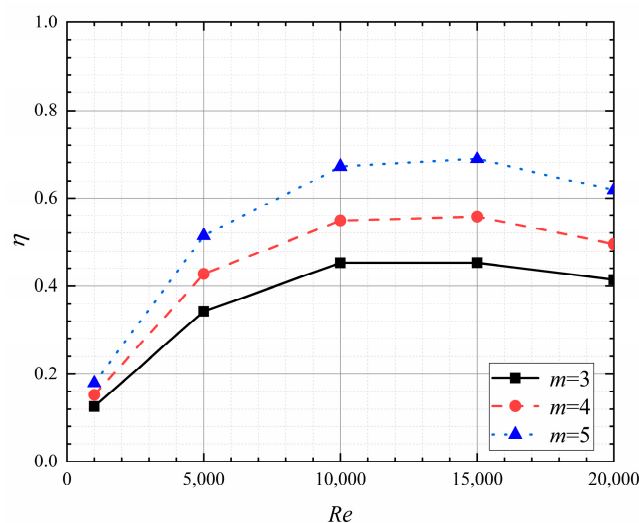

Figure 16. Variation of thermal enhancement factor with Re number.

4.4. Anti-Clogging Performance

One main issue that must be considered in tree-like bifurcating microchannel networks is the potential clog of fluid flow in the channels. It should be taken into account that obstruction, which may be brought by particulate or impacting foreign bodies can be hazardous for the cooling system. Dendritic arrangements enable the maintenance of cooling in the event of damage to the turbine blade; therefore, it is essential to study the effects of possible blockage in tree-like branching microchannels.

The locations of clog occurring in the tree-like bifurcating microchannel network for $m = 3$, 4, and 5, labelled with serial numbers ①–⑤, are demonstrated in Figure 17. The predicted velocity vector distributions over the mid-plane ($z = 0.5H$) for $m = 5$ at three blockage place ($BL = 2$, 3, and 5) are shown in Figure 18a–c, respectively. In the context of branch and confluence structures, the cooling channels are connected to one another at specific joints and flow separately from one another in other regions. Compared to the flow pattern in the tree-like bifurcating microchannel network without blockage, the flow characteristics show a difference in the networks with blockage, regardless of where it occurs. As can be seen from the figure, the airflow velocity decreases to zero in the blocked channel. However, the fluid flow acceleration happens in the surrounding area due to the flow compensatory mechanism.

Figure 19a–c displays the temperature distributions over the mid-plane. It has been found that the temperature distribution in the area covered by a branching microchannel network does not change significantly. In the blocked region, the temperature has not risen up much because the heat transfer capability in the surrounding sub-channels get improved by increasing the fluid velocity. Compared to the temperature over the mid-plane of the unobstructed case, the mean temperature is, respectively, higher by approximately 10.1 K, 11.2 K, and 10.8 K in the cases for $BL = 2$, 3, and 5.
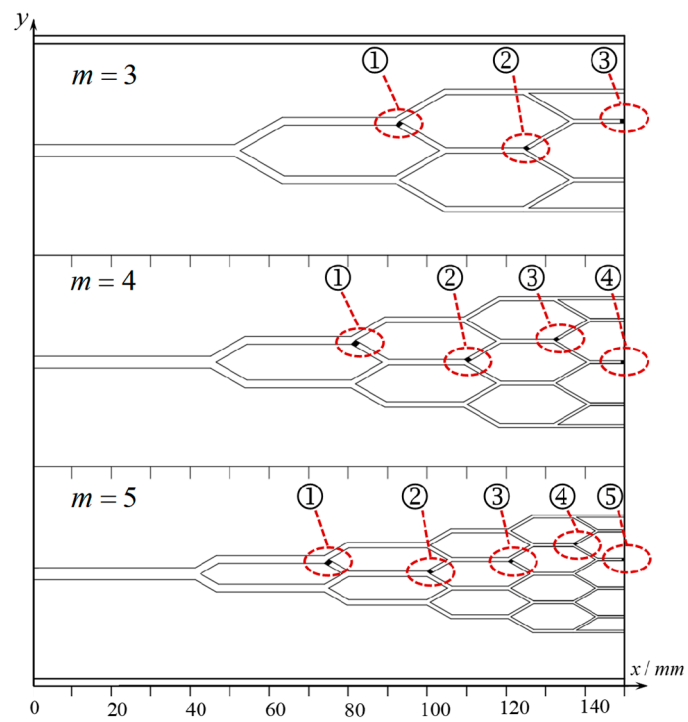
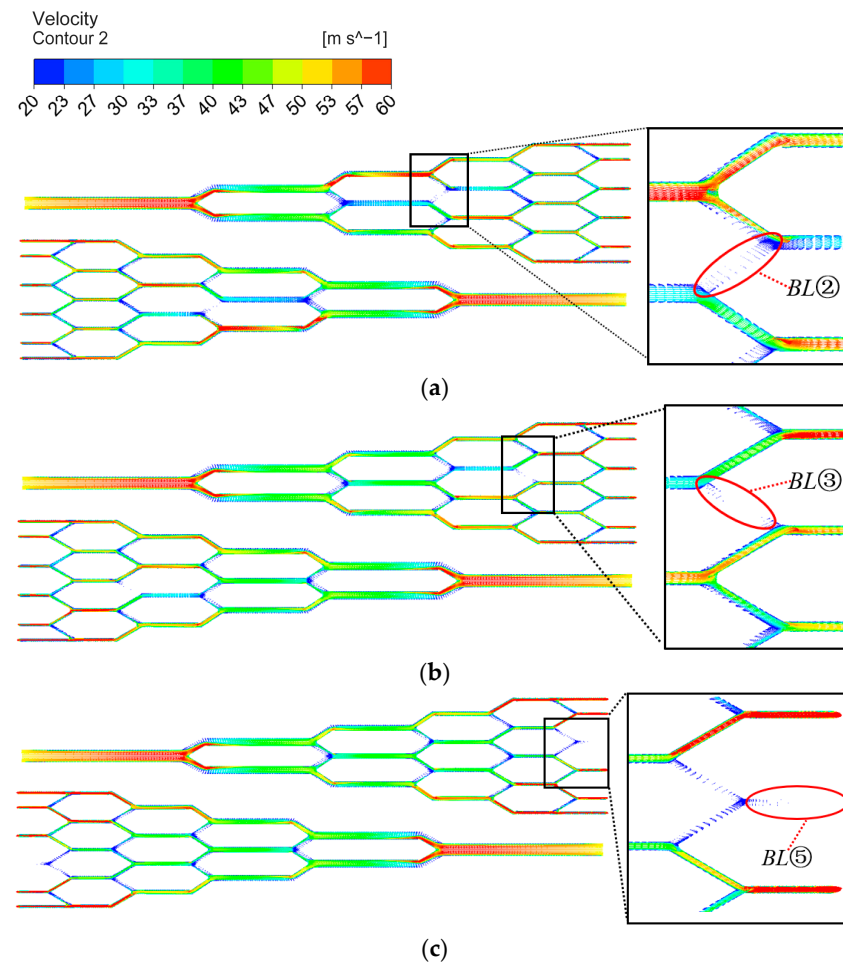**Figure 17.** Two-dimensional view of the blockage locations (*BL*) for *m* = 3, 4, and 5.

Figure 18. Velocity vector distribution over mid-plane (*z* = 0.5*H*) at (**a**) *BL* = 2, (**b**) *BL* = 3, and (**c**) *BL* = 5 for *m* = 5.
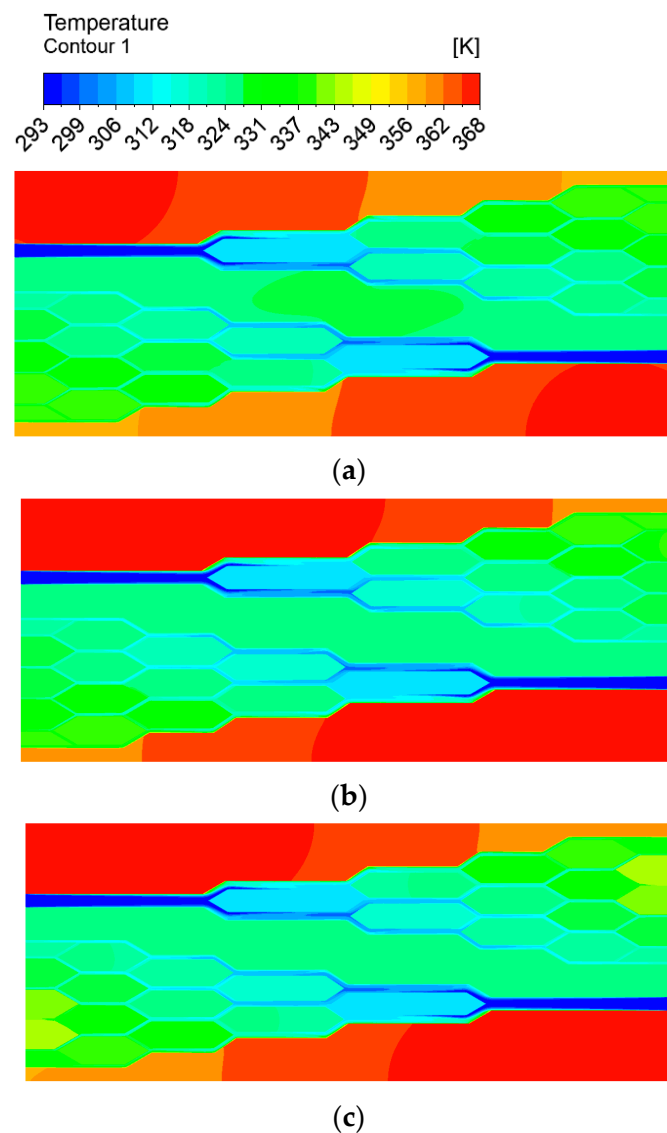
Figure 19. Temperature distribution over mid-plane ($z = 0.5H$) at (**a**) $BL = 2$, (**b**) $BL = 3$, and (**c**) $BL = 5$ for $m = 5$.

Figure 20a,b present the maximum temperature variations over the mid-planes of blockage at different locations and branching levels at $Re = 10,000$ and 20,000, respectively. It is worth noting that T_{max} for the case without blockage is about 355.3 K, 353.3 K, and 355.3 K for $m = 3, 4, 5$ at $Re = 10,000$. Nevertheless, the maximum temperature rises to 450 K, 434.9 K, and 401.4 K for the case with $BL = 1$, and to 426.3 K, 409.7 K, and 399.2 K for the case with $BL = 3$. When the Re number increases to 20,000, the maximum temperatures for all the cases are decreased. In general, the predicted maximum temperature ascends up when the sub-channel is blocked, especially for the channels at the low-order branching level, which are higher than those in the high-order branching level. However, the phenomenon of maximum temperature changing with the branching level is more obvious in the branching microchannel for $m = 3$. The influence brought by the location of blockage on the temperature distribution declines with an increase in m and Re number. By combining Figure 19, it is clear that T_{max} appears at two opposite corners of the region that cannot be covered by the microchannel network. Despite all the blocked scenarios, the local temperature of the covered region by the cooling tree-like branching microchannel network remains lower than the uncovered region due to the compensation effect of the adjacent branched channel.
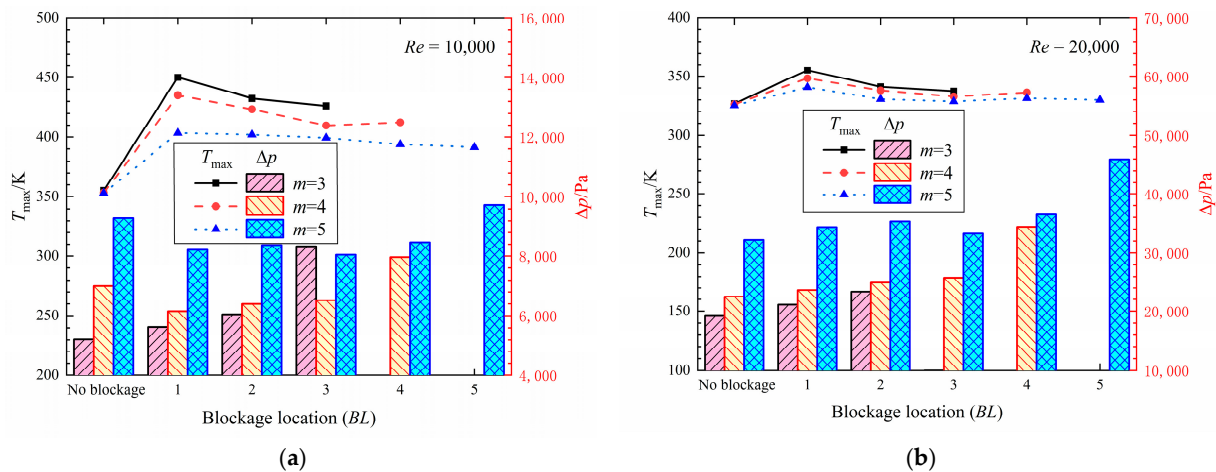
Figure 20. The variations in the maximum temperature and pressure drop of the tree-like branching microchannels with and without blockage at (**a**) *Re* = 10,000 and (**b**) *Re* = 20,000.

The pressure drop, which changes with the location of blockage, is also shown in Figure 20. It is can be seen that the pressure drop shows an increase in tree-like bifurcating microchannels as the *m* and *Re* numbers increase. The blocked channels at a high-order branching level exhibit a higher pressure drop, especially when the outlet of the sub-segment channel is blocked. The maximum increase in pressure drop ratio is about 59%, observed at *BL* = 3 for *m* = 3 when *Re* = 10,000. However, when obstruction occurs at specific locations, such as *BL* = 1 for *m* = 4 and *BL* = 2 for *m* = 5, the pressure drop is even lower than in the unobstructed channel due to the effect of flow compensation. In general, the tree-like branching microchannel shows better anti-clogging performance with a greater total number of branching levels.

5. Conclusions

In this study, a tree-like branching microchannel with bifurcating interconnections was designed as an innovative internal cooling configuration for gas turbine blades. The influence of *m* and the effects of channel blockage on the flow field and heat transfer characteristics were investigated through theoretical analysis, experiment, and numerical simulations.

Compared to the conventional parallel channel network, the tree-like bifurcating network has better heat transfer and hydrodynamic performance by adopting the method of theoretical analysis. The total heat transfer ratio and pressure drop ratio are closely related to the structure parameters. A larger ratio of L_b/L_0, total number of the branching levels *m*, or fractal dimension *D* are all observed to result in stronger heat transfer capability but also require a pumping power penalty.

The results of verification experiments reveal that the turbulence model of SSG can adequately and accurately predict heat transfer and flow details. Additionally, the experimental and numerical data of heat transfer coefficients match well with Stephan's and Shah's correlations. In comparison of the classic correlation value, the experimental and numerical friction factors are lower in the turbulent region, and show a decreasing tendency as *Re* < 11,000. They gradually rise when the *Re* number increases continuously.

The results of comparison with three branching levels show that as the *Re* number increases from 1000 to 20,000, Nu/Nu_s increases, f/f_s decreases initially until *Re* = 10,000 and then rises, and η ascends when *Re* < 15,000, and then gradually declines. Furthermore, Nu/Nu_s, f/f_s and η are increased when *m* increases from 3 to 5.

A tree-like branching microchannel with branches interconnected can decrease the risk of thermal damage caused by flow clogging. With the increase of *m* and *Re* number, the impact of blockage on the heat transfer performance is reduced. These results reveal the

robustness of tree-like microchannel networks for gas turbine blade cooling, which requires high reliability.

Nomenclature

c	constant	$\dot{Q}$	the total heat removed by air
D	ractal dimension of channel length distribution	Q_h	total convective heat transfer of bifurcating channels
d_0	the 0th channel hydraulic diameters		total convective heat transfer of parallel channels with
d_k	the kth channel hydraulic diameters	Q_{hp1}	the same heat transfer area as bifurcating channels and
f	the Fanning friction factor		diameter of d_0
f_s	friction factor in the smooth channel	Q_{hp2}	convective heat transfer of parallel channels
h_k	heat transfer coefficient of the kth level channel	S	the total heat transfer area of a tree-like net
L_b	the channel length of the oblique channel	S_k	the total heat transfer area of the kth level channel
L_0	the channel length of the 0th branching level	S_{p2}	total heat transfer area of parallel channels
L_k	the channel length of the *k*th branching level	T_{in}	the air mean temperature of the inlet in the branching microchannel
L	the centerline length from the channel inlet to the outlet	T_{out}	the air mean temperature of the outlet in the branching microchannel
L_{ak}	the channel length of the straight channel after bifurcation	$\dot{V}$	channel volume flow rate of air
m	the total number of branching levels	v_0	velocity in the initial channel
Nu_s	the averaged Nu number in a smooth microchannel for a fully developed flow	v_k	velocity in the kth level channel
n	number of parallel channels	β	the ratio of the diameter of the channel at the (k + 1)th branch level versus the diameter of the channel at the kth branch level
N	number of branches into which a single channel bifurcates	α	the ratio of the length of the channel at the (k + 1)th branch level versus the length of the channel at the kth branch level
P	pumping power of the tree-like channels		
P_{p2}	pumping power of parallel channels	Δ	fractal dimension of the hydraulic diameter distribution
Q	flow rate		
Q_{p2}	flow rate of parallel channels	λ	the mass-averaged thermal conductivity of air
Δp_f	The pressure drop of the tree-like channels	ΔT	temperature difference
Δp_{p2}	The pressure drop of the parallel channels		

References

1. Takeishi, K. Evolution of Turbine Cooled Vanes and Blades Applied for Large Industrial Gas Turbines and Its Trend toward Carbon Neutrality. *Energies* **2022**, *15*, 8935. [CrossRef]
2. Ahn, J. Large Eddy Simulation of Flow and Heat Transfer in a Ribbed Channel for the Internal Cooling Passage of a Gas Turbine Blade: A Review. *Energies* **2023**, *16*, 3656. [CrossRef]
3. Ren, Z.; Yang, X.; Lu, X.; Li, X.; Ren, J. Experimental Investigation of Micro Cooling Units on Impingement Jet Array Flow Pressure Loss and Heat Transfer Characteristics. *Energies* **2021**, *14*, 4757. [CrossRef]
4. Lee, C.-S.; Shih, T.I.-P.; Bryden, K.M.; Dalton, R.P.; Dennis, R.A. Strongly Heated Turbulent Flow in a Channel with Pin Fins. *Energies* **2023**, *16*, 1215. [CrossRef]
5. Yang, Y.; Du, J.; Li, M.; Li, W.; Wang, Q.; Wen, B.; Zhang, C.; Jin, Y.; Wang, W. Embedded microfluidic cooling with compact double H type manifold microchannels for large-area high-power chips. *Int. J. Heat Mass Transf.* **2022**, *197*, 123340. [CrossRef]

6. He, Z.; Yan, Y.; Zhao, T.; Zhang, L.; Zhang, Z. Multi-objective optimization and multi-factors analysis of the thermal/ hydraulic performance of the bionic Y-shaped fractal heat sink. *Appl. Therm. Eng.* **2021**, *195*, 117157. [CrossRef]

7. Kizilova, N.; Sauermoser, M.; Kjelstrup, S.; Pollet, B.G. Fractal-like flow-fields with minimum entropy production for polymer electrolyte membrane fuel cells. *Entropy* **2020**, *22*, 176. [CrossRef] [PubMed]

8. Barnoon, P. Numerical assessment of heat transfer and mixing quality of a hybrid nanofluid in a microchannel equipped with a dual mixer. *Int. J. Thermofluid* **2021**, *12*, 100111. [CrossRef]

9. Jing, D.L.; Zhan, X.K. Cross-sectional dimension dependence of electroosmotic flow in fractal treelike. *Micromachines* **2020**, *11*, 266. [CrossRef]

10. Hu, B.; Wang, J.; Ma, Z.; Sang, S. Permeability and thermal conductivity models of shale matrix with a bundle of tortuous fractal tree-like branching micropore networks. *Int. J. Therm. Sci.* **2021**, *164*, 106876. [CrossRef]

11. Saleh, B.; Sundar, L.S. Experimental study on heat transfer, friction factor, entropy and exergy efficiency analyses of a corrugated plate heat exchanger using Ni/water nanofluids. *Int. J. Therm. Sci.* **2021**, *165*, 106935. [CrossRef]

12. Tian, Y.; Liu, X.; Xu, Q.; Luo, Q.; Zheng, H.; Song, C.; Zhu, Z.; Gao, K.; Dang, C.; Wang, H.; et al. Bionic topology optimization of fins for rapid latent heat thermal energy storage. *Appl. Therm. Eng.* **2021**, *194*, 117104. [CrossRef]

13. Bjan, A. *Shape and Structure, from Engineering to Nature*; Cambridge University Press: Cambridge, UK, 2000. [CrossRef]

14. Bejan, A. Constructal Law: Optimization as Design Evolution. *J. Heat Trans.* **2015**, *137*, 061003. [CrossRef]

15. West, G.B.; Brown, J.H.; Enquist, B.J. A General Model for the Origin of Allometric Scaling Laws in Biology Science. *Science* **1997**, *276*, 122–126. [CrossRef] [PubMed]

16. Senn, S.M.; Poulikakos, D. Laminar mixing, heat transfer and pressure drop in tree-like microchannel nets and their application for thermal management in polymer electrolyte fuel cells. *J. Power Sources* **2004**, *130*, 178–191. [CrossRef]

17. Alharbi, A.Y.; Pence, D.V.; Cullion, R.N. Thermal characteristics of microscale fractal-like branching channels. *J. Heat Transf.* **2004**, *126*, 744–752. [CrossRef]

18. Chen, Y.P.; Yao, F.; Huang, X.Y. Mass transfer and reaction in methanol steam reforming reactor with fractal tree-like microchannel network. *Int. J. Heat Mass Transf.* **2015**, *87*, 279–283. [CrossRef]

19. Chen, Y.P.; Cheng, P. Heat transfer and pressure drop in fractal tree-like microchannel nets. *Int. J. Heat Mass Transf.* **2002**, *45*, 2643–2648. [CrossRef]

20. Rubio-Jimenez, C.A.; Hernandez-Guerrero, A.; Cervantes, J.G.; Lorenzini-Gutierrez, D.; Gonzalez-Valle, C.U. CFD study of constructal microchannel networks for liquid-cooling of electronic devices. *Appl. Therm. Eng.* **2016**, *95*, 374–381. [CrossRef]

21. Jing, D.L.; Song, J. Comparison on the hydraulic and thermal performance of two tree-like channel networks with different size constraints. *Int. J. Heat Mass Transf.* **2019**, *130*, 1070–1074. [CrossRef]

22. Lu, Z.H.; Zhang, K.; Liu, J.X.; Li, F. Effect of branching level on the performance of constructal theory based Y-shaped liquid cooling heat sink. *Appl. Therm. Eng.* **2020**, *168*, 114824. [CrossRef]

23. Wang, X.Q.; Yap, C.; Mujumdar, A.S. Laminar Heat Transfer in Constructal Microchannel Networks with Loops. *J. Electron. Packag.* **2006**, *128*, 273–280. [CrossRef]

24. Wang, X.Q.; Mujumdar, A.S.; Yap, C. Thermal characteristics of tree-shaped microchannel nets for cooling of a rectangular heat sink. *Int. J. Therm. Sci.* **2006**, *45*, 1103–1112. [CrossRef]

25. Xu, P.; Wang, X.Q.; Mujumdar, A.S.; Yap, C.; Yu, B.M. Thermal characteristics of tree-shaped microchannel nets with/without loops. *Int. J. Therm. Sci.* **2009**, *48*, 2139–2147. [CrossRef]

26. Miao, T.J.; Chen, A.M.; Xu, Y.; Yang, S.S.; Yu, B.M. Optimal structure of damaged tree-like branching networks for the equivalent thermal conductivity. *Int. J. Therm. Sci.* **2016**, *102*, 89–99. [CrossRef]

27. Devore, M.A.; Kaufman, E.D. Branched Airfoil Core Cooling Arrangement. U.S. Patent 8449254, 28 May 2013.

28. Ahmad, F.; Burzych, T.; Hummel, E. Arrangement of Cooling Channels in a Turbine Blade. U.S. Patent 15023392, 17 September 2014.

29. Shui, L.Q.; Huang, B.; Dong, K.K.; Zhang, C.Y. Investigation of Heat Transfer and Flow Characteristics in Fractal Tree-Like Microchannel With Steam Cooling. In Proceedings of the ASME Turbo Expo 2017: Turbomachinery Technical Conference and Exposition, Charlotte, NC, USA, 26–30 June 2017. [CrossRef]

30. Shui, L.; Huang, B.; Gao, F.; Rui, H. Experimental and numerical investigation on the flow and heat transfer characteristics in a tree-like branching microchannel. *J. Mech. Sci. Technol.* **2018**, *32*, 937–946. [CrossRef]

31. Xu, P.; Yu, B. The scaling laws of transport properties for fractal-like tree networks. *J. Appl. Phys.* **2006**, *100*, 104906. [CrossRef]

32. Hylton, L.D.; Nirmanlan, V.; Sultanian, B.K.; Kaufman, R.M. The Effects of Leading Edge and Downstream Film Cooling on Turbine Vane Heat Transfer; NASA CR-182133. 1988. Available online: https://ntrs.nasa.gov/citations/19890004383 (accessed on 17 July 2023).

33. Stephan, K.; Preußer, P. Wärmeübergang und maximale Wärmestromdichte beim Behältersieden binärer und ternärer Flüssigkeitsgemische. *Chem-Ing-Tech* **1979**, *51*, 37. [CrossRef]

34. Kline, S.J.; McClintock, F.A. Describing experimental uncertainties in single-sample experiments. *Mech. Eng.* **1953**, *75*, 3–8.

35. Shah, R.K.; London, A.L. Laminar Flow Forced Convection in Ducts. *J. Fluids Eng.* **1978**, *102*, 431–455. [CrossRef]

36. Incropera, F.P.; De Witt, D.P. *Fundamentals of Heat and Mass Transfer*, 2nd ed.; John Wiley and Sons: New York, NY, USA, 2007.

37. Kakac, S.; Shah, R.K.; Aung, W. *Handbook of Single-Phase Convective Heat Transfer*; John Wiley and Sons: New York, NY, USA, 1987.